Atomic size effect on critical cooling rate and glass formation

Payman Jalali and Mo Li
School of Material Science and Engineering, Georgia Institute of Technology, Atlanta, Georgia 30332, USA
(Received 10 November 2003; revised manuscript received 30 September 2004; published 21 January 2005)

Atomic size effect on critical cooling rate and glass formability in a model binary system is investigated using molecular dynamics simulation. To isolate atomic size effect from the rest of the factors that critically influence the glass formation, a hard sphere model is employed in conjunction with a newly developed densification method. The glass formability is defined as a set of optimal conditions that result in the slowest cooling rate of the glass-forming liquid. Critical cooling rates are identified from extensive molecular dynamics simulations. A kinetic glass-forming diagram is mapped out that marks the boundary between the glass-forming regions and competing crystalline phases in terms of the parameters of the atomic size ratio and alloy concentration. It is found that the potency of the atomic size difference on glass formation is influenced greatly by the competing metastable and equilibrium crystalline phases in the system, and the kinetic processes leading to the formation of these phases. The mechanisms of the atomic size effect on topological instability of crystal packing and glass formation are discussed.

DOI: 10.1103/PhysRevB.71.014206 PACS number(s): 61.25.Mv, 81.05.Kf, 61.20.Ja, 61.43.Fs

I. INTRODUCTION

Glass form ability (GFA), or glass formability, is the measure of how easy a given material system can be made into glass. GFA is usually quantified by the cooling rate required to make a glass from the liquid. A better or easier glass former is the system that requires slower cooling rate. There are also several other measures widely used to gauge metallic glass formability. These criteria are featured in their connection to other material properties. One is Turbull's reduced glass transition temperature $T_{\mathrm{RG}}=T_g/T_m$,[1] where T_g is the glass transition temperature and T_m is the melting temperature of the corresponding glass-forming system. Another is the difference between the crystallization temperature and the glass transition temperature $\Delta T=T_x-T_g$.[2] As pointed out by Turnbull, a good glass former is the one of which the critical T_{RG} equals to or becomes larger than $2/3$. Otherwise, crystal nucleation prevails during cooling, which pre-empties the glass formation. On the other hand, ΔT measures the temperature window between the glass transition and the first crystallization when a glass is heated up from below. High values of ΔT usually indicate more stable undercooled liquids. Clearly these two criteria attempt to measure the same glass formability using different references with respect to T_g: The critical T_{RG} uses melting point T_m of the glass-forming liquids as a reference and ΔT uses the crystallization temperature T_x. Recently a new criterion is proposed[3] that takes both T_m and T_x as the reference.

Both criteria are connected, though implicitly, to kinetics of glass-forming liquid: a high T_{RG} implies that T_g is closer to T_m, thus a slow cooling rate is attainable when the liquid is cooled across the narrower temperature gap T_m-T_g; larger ΔT also indicates a slower cooling rate as the undercooled liquid can be kept longer below T_x. Therefore, slow cooling rate is indicative of a better GFA: The better the GFA is, the lower the required cooling rate for a glass-forming liquid, and larger or more bulky a glass sample can be made.[2]

Indeed, a large number of good glass-forming systems obey these criteria.[1–3] But many exceptions also occur, especially in some of the bulk metallic glass systems synthesized recently.[4] The deviations from these rules call for a close examination of the glass formability and, most importantly, discovery of the underlying mechanisms of the glass formation. On the practical side, it is highly desirable to establish a set of new criteria that can *predict* the glass formability from intrinsic material properties before any glass is made, as the parameters such as T_g, T_m, or T_x used are the properties measured from the glass samples already made.

A handful of such intrinsic material properties have been identified that are known to affect the glass formability effectively. They are (1) the heat of mixing of different alloy elements ΔH, (2) the atomic size difference, or atomic size ratio, α, (3) the number of alloy composition n, and (4) the relative concentration of each of the alloy elements $x_1, x_2, \ldots, x_{n-1}$. For example, nonpositive heat of mixing is needed to ensure the stability of the glass-forming liquid. Increasing number of alloy components seems to lead to better glass formers.[5] However, the precise mechanisms of how these material properties affect the glass formability have not been fully apprehended.

As a result, the glass formability is still determined based on the derivative properties such as T_g, T_m, or T_x.[1–3] Synthesis of metallic glasses remains an empirical process: A large number of alloys are prepared by trial and error; and thermal and structural analysis is performed on the samples. Then the abovementioned criteria are tested using the data from the measurements. Although the output from the testing against the criteria can be used as an important intermediate step to guide the search of better glass formers in a large number of cycles of trial and error, the lack of an effective, *a priori*, or intrinsic-material-property-dependent criterion greatly limits our ability to predict and discover new bulk metallic glass systems.

In this paper, we shall study one of the factors, the atomic size difference. It is one of the intrinsic material properties known to affect the glass formability critically. Experiments show that the glass formation is easier if the atomic size differences of the selected alloy elements are larger than

12–15 %.[6] It is also a common practice in computer simulations to use systems made of atoms or particles of different sizes to enhance glass formation. This empirical relation between the atomic size difference and glass formability, however, has not been explored theoretically as much as it should be. Only a semiquantitative relation is available[7,8] that connects the minimum alloy concentration for the glass formation and the atomic size difference. Glass-forming regions in binary systems are predicted using this model. A large number of transition metal or refractory metal binary systems are shown to follow the trend predicted by this model.[7,8] But many exceptions also occur, which include binary systems made of metal/metalloid and rare-earth/transition-metal atoms. They are known to have large charge transfer during mixing. Even within the binary systems that follow the general trend predicted by the relation, the deviations in the calculated minimum alloy concentrations from known experimental ones are typically in the range of 5–80 %.[7]

Mixing solute atoms of different atomic sizes with the host atoms introduces packing incompatibility (in crystalline phase) and as a result, local atomic stress arises. If the fluctuation of the local pressure caused by the atomic size difference reaches a critical value, the local coordination number of the atom with different atomic size from its neighbors will prefer to have local packing of noncrystalline symmetry, thus resulting in glass formation. This mechanism proposed by Egami and Waseda has implicitly the substitutional solid solution in mind.[7,8] A recent extension of this model considers alloy elements that could sit in the interstitial sites of the host crystal structures.[9] The atomic size disparity of the interstitial atoms with the host atoms leads to another bound in the glass formation region ($0.60<\alpha<0.80$). However, the atomic size ratio of most pairs of atoms in the periodic table is usually in the range of 0.7–1.3 for majority of metal atoms. Only very limited number of binary systems with at least one transition or refractory metal atom falls into this region ($\alpha<0.70$). This new bound, therefore, has very restricted application in glass-forming systems of transition and refractory metals. But many nonmetallic glass-forming systems have different sized constitutive particles such as in colloids, granular particles, and minerals. In these systems, particle size can vary freely.

Egami-Waseda model captures some trend of the effect of atomic size difference on the glass formation. Due to the complexity of the problem, detailed mechanisms of how atomic size difference affect topological packing and glass formation still remain unsettled, especially those pertinent to *kinetics* of glass-forming liquids. For example, what is its connection to the cooling rate of the glass-forming liquids? How does the atomic size difference affect glass formability if multiple stable and metastable crystalline phases are in direct competition with glass phase? Answers to those issues which are not considered in the previous models, are expected to further our understanding of glass formability and also contribute to establishment of a truly predictive criterion for glass synthesis.

To answer these questions, we carry out an investigation using molecular dynamics (MD) simulations. The advantage and uniqueness of this approach will become clear as our work progresses in this paper. Specifically, we employ a hard sphere model to probe the effects of only atomic size difference on the glass formability, which is impossible to do in experiment. With the help of a discontinuous densification method in the MD simulation, we are able to identify the critical cooling rates of the binary hard sphere system as a function of the atomic size ratio and alloy concentration. We also characterized various metastable and stable crystalline phases and chemical clustering formed during cooling of the glass-forming liquids that are competing with glass formation. From the structure analysis of these crystalline phases and clusters, we could infer the changing potency of the atomic size effect on glass formability. Finally, we mapped out a kinetic diagram of glass formation from these simulations. It marks the boundary of a glass-forming region in the parameter space of the atomic size ratio and alloy concentration.

This paper is organized as follows. In the next section, we outline the simulation methods and the model hard sphere system used in our simulation. In Sec. III, we describe the results obtained from our simulations of a binary hard sphere system, including the critical cooling rate, the lowest critical cooling rate, crystalline phase formation, possible mechanisms of local packing instability caused by atomic size difference, the limitations of the instability models, and the kinetic diagram for glass formation. In Sec. IV, we discuss the relations between crystalline phase and the glass formation. Finally, we summarize our work in Sec. V.

II. MODEL SYSTEM AND SIMULATION METHODS

The model material used in this study is a hard sphere (HS) system. Atoms in this model are represented as hard spheres. Different from the systems with continuous interatomic potentials, such as Lennard-Jones or embedded atom potentials, atoms or particles in HS systems interact with a potential $V(r_{ij})$ that is purely repulsive,[10] that is, $V(r_{ij})=\infty$ if $r_{ij}\leqslant(d_i+d_j)/2$, and $V(r_{ij})=0$, otherwise. r_{ij} is the separation distance between atom i and j in the system; d_i and d_j are their diameters, respectively. Therefore, a multicomponent system made of hard spheres of different sizes has zero enthalpy of mixing. This choice of the model system is made deliberately to single out the atomic size factor from the rest of the intrinsic material properties, as it is known that mixing different types of atoms introduces not only different atomic diameters but also different enthalpies of mixing. The hard sphere model system allows us to focus on the effects of atomic size only.

For binary hard sphere model, there are only two parameters that can fully characterize the system. One is the atomic size ratio, $\alpha=d_B/d_A$, and the other is the relative concentration of the alloy element $x_B=N_B/(N_A+N_B)$, where d_A and d_B are the atomic diameters of type A and B, and N_A and N_B are the number of each type of the atoms. $N=N_A+N_B$ is the total number of atoms in the system. In the rest of this paper, we shall call the type-B atom the solute atom, or alloy element, and the type A atom the host, or solvent atom. The solute is the minority element ($x\leqslant 0.50$) and the solvent is the majority element. Their names can switch if the solute becomes majority, as we see later in this work.

The simulation technique of this hard sphere model system is correspondingly different from that of the systems with continuous interatomic interactions. Instead of solving the equations of motion for atoms in a series of discrete time steps as in the standard MD simulations, the changing positions, and velocities of the hard spheres are acquired through the events of collision. The collision time of a pair of atoms is obtained when the separation of two atoms approaches the sum of their radii $r_{ij}=(d_i+d_j)/2$. Two different techniques are used to determine collision partners of each sphere.[10] In one technique, we assign an array for each particle that contains the list of its neighbors up to the kth nearest neighbors. This neighbor list is modified periodically depending on how fast the neighbors change. The value of k is usually 2 or 3, which depends on the instantaneous packing density of system. For a very dilute system, k may be increased to 5 or 6, while it can be 1 for a jammed state. Obviously the updating period of neighbors list affects the efficiency of the algorithm.[10] In the second technique, we implement linked cell structure to determine the collision partners of particles. Each particle belongs to a cell and its collision partners are searched within this cell and the neighboring cells.[10,11] These techniques can reduce the number of calculations considerably and larger systems can thus be handled. To avoid unnecessary digression from the main theme of this paper, we leave the technical details of the algorithm and computation efficiency in a separate publication.[12] We only give a brief description of the algorithm used in this work below.

Another special feature of these simulations is modeling quench process. For hard sphere systems, temperature is not defined independent of other state variables. In fact, it is directly related to the packing density of the system.[13] Therefore, quenching a hard sphere liquid is the same as increasing the packing density. For this reason, we use "quench" and "densification" synonymously. In this study we adopted a discontinuous densification algorithm that allows us to quench a liquid but avoid trapping the system as much as possible in artificial metastable states. So the equilibrium as well as metastable crystalline phases can be obtained reliably.

The central idea of this algorithm is to increase the sphere diameters in a controlled fashion, which is equivalent to increasing the packing density while keeping the volume of the simulation box fixed. During a quench or densification process, we increase the diameters of the atoms, usually after a given time interval. The amount of radius growth is not a constant at each step; it depends on the minimum separation distance between two atoms available in the system at the instant. We consider a binary system below. The same formulation can be extended straightforwardly to monatomic as well as multicomponent systems.

Suppose that at a given time, the minimum surface-surface distance $d_{\min}$ is found between atoms i and j of diameter d_i and d_j in the system. Their new diameters will be assigned using the following relations to assure that the original size ratio will not change:

$$d_i' = d_i + \delta d_i, \tag{1a}$$

$$d_j' = d_j + \delta d_i/\alpha_{ij}. \tag{1b}$$

The size ratio between atom i and j is denoted by α_{ij}, that is, $\alpha_{ij}=d_i/d_j=d_i'/d_j'$. The size increment δd_i is a fraction of the surface-surface distance $d_{\min}$, $\delta d_i=f[d_i/(d_i+d_j)]d_{\min}$. The value of the coefficient f can be chosen between 0 and 2, as it is not desirable for the size growth to introduce any overlapping between the spheres. In the present simulations f is set to 0.9. Once the size increments, δd_i and $\delta d_j=\delta d_i/\alpha_{ij}$ are determined for the two types of atoms i and j, the diameters of the rest of atoms of the same type will be changed by the corresponding amount while the size ratio is maintained. So in a quenching process, the diameters of the atoms with different sizes remain constant up to time t_s and then they jump to new values. They subsequently remain constant until the next step which is determined again by the available minimum separation $d_{\min}$. Note that t_s controls the densification rate. Larger values of t_s correspond to smaller densification rates. The mean quench rate is determined by the mean growth rate of packing density of the system within a time interval made of 10-20 such steps.

Each simulation starts with N number of spheres, typically $N=500-20\,000$ in this work, which are distributed in a low-density (or liquid) configuration. An initial quench rate is chosen for each system characterized by different atomic size ratio and concentration (α, x_B). The system is subsequently quenched to higher density. Different quench rates can be implemented in the simulation for each given system. A high quench rate usually leads to glass formation. As shown in the next section, by varying the quench rate, we can identify the critical quench rate crossing which crystalline and glass phase boundary is traversed. The critical quench rate thus identified is the slowest cooling rate that represents materials' GFA.

Note that in the algorithm we adopt here, the diameters of spheres increase (a) discontinuously and (b) based on instantaneous minimum atomic distance. These provide extra chance for relaxation of atoms during densification as compared to previously used algorithms. This can be observed in Fig. 1(a) in which the rate of packing density growth decreases beyond certain time (or packing density) due to the decrease in the minimum atomic distance at higher packing densities. A previously used densification algorithm[14] with constant rate of diameter growth introduces an increasing rate of packing density growth in time, as shown in Fig. 1(a). This will add additional, undesirable forces for overlapping atoms and therefore, causes the system to evolve unnaturally toward glass transition, and in particular, crystallization, while our present algorithm does not do so.

To map out the kinetic diagram for glass formation (Fig. 3), we have run several hundreds of samples for different combinations of atomic size and solute concentration. Each sample is simulated with 5–10 different quench rates [see Fig. 1(b)]. Each simulation lasts several million collisions. Data are collected at the end of the simulations and various measures are taken later to characterize structures of the binary systems during and after quenching. Among them are radial distribution functions, the bond orientational order distribution function, the nearest-neighbor number distribution

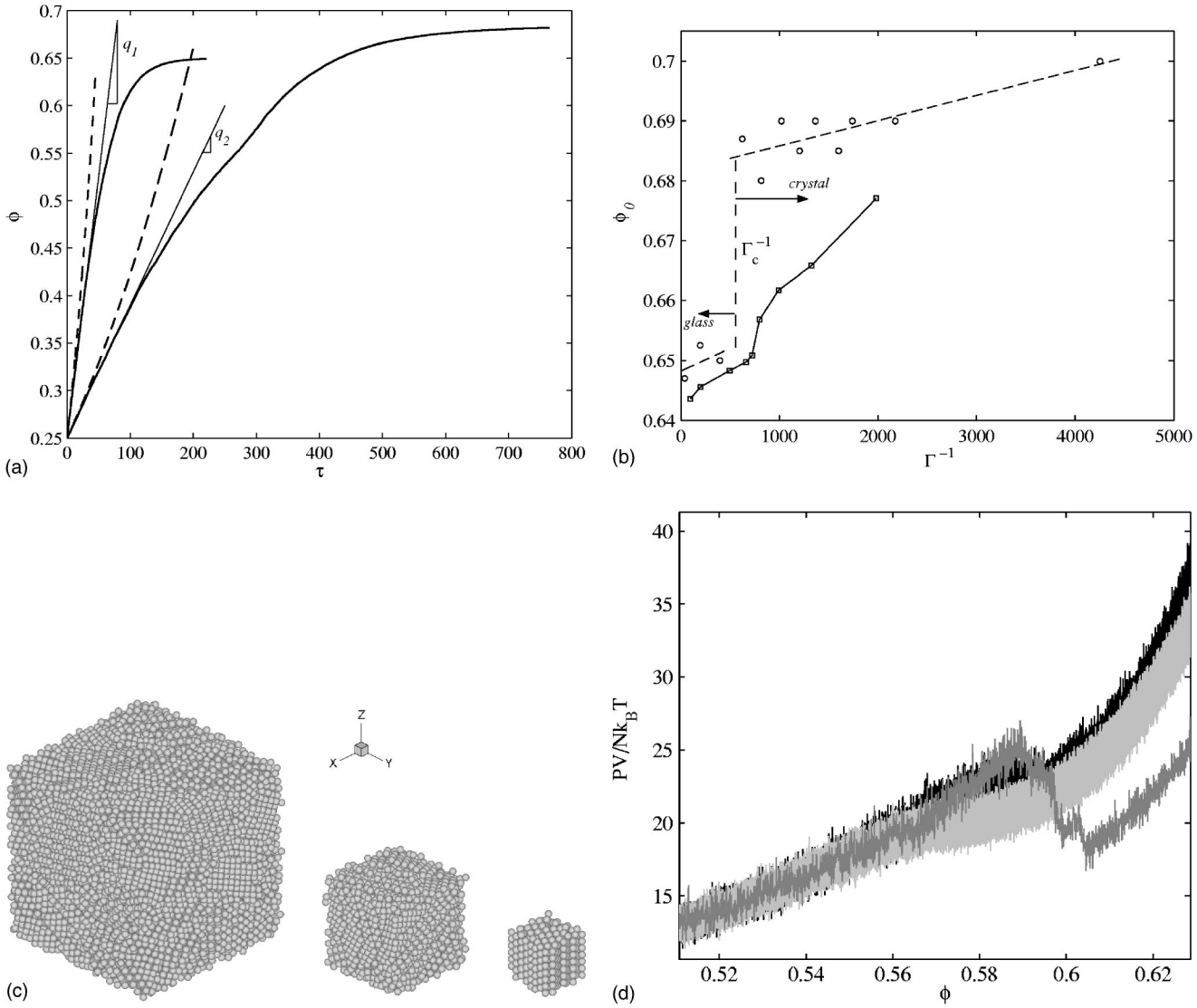

FIG. 1. (a) Variation of packing density versus time with different initial densification rates. The fast densification has the initial rate of $q_1=0.0055$ and the slow densification has $q_2=0.0014$. Solid lines represent the results of the current simulations and dash lines represent φ-τ curves using the protocol introduced in Ref. 14. Thin solid lines show the initial slope of the curve in our simulation. (b) Dependence of the final packing density on initial quench, or densification (Ref. 16) rate (Γ^{-1}) in a one-component system. Our cooling rate q is related to Γ by $q=(\sigma^2 N\pi/2\sqrt{\sigma^3/T_r})\Gamma$. N is the number of spheres in the periodic box, σ is their dimensionless diameter, and T_r represents a reduced temperature defined based on dimensionless velocity of spheres. We prefer to use q rather than Γ as it is a general definition that can be readily used in binary and polydisperse packing. Each circle represents one MD simulation of the system at a specific quench rate. 500 spheres placed in a cubic box are used. The critical densification rate is $q_c=0.00453$. The sharp division of the crystal and glass phase region can be seen. Results of a continuous size growth algorithm (Ref. 16) is also shown by squares connected by solid line. (c) Quenched samples consisted of different number of spheres (20 000, 3000, and 500). All samples are obtained around their CCR, which is $q_C=0.0039$ with 10% variation. (d) Variation of PV/Nk_BT with φ for the cases shown in Fig. 1(c). Black, light gray and dark gray colors represent samples with 20 000, 3000, and 500 hard spheres.

function, as well as visualization. Another method for detecting phase transition in each simulation is to plot the equation of states, PV/Nk_BT versus the packing density φ, where P and V are pressure and volume of the system, and k_B is the Boltzmann constant and T is the system temperature. If crystallization occurs, a sharp drop can be observed in PV/Nk_BT at the transition packing density. This transition packing density is around 0.56 for monodisperse packing, but it may vary from 0.55 to 0.59 in binary mixtures.

Since the critical quench rate is measured through crystallization, possible effects from finite sample size need to be checked. In this work, we used three sample sizes 500, 3000, and 20 000, to test the finite size effect. The variation of the critical quench rates is found less than 10% for a variety of mixtures ($\alpha \geqslant 0.2$) with different sample sizes. This agrees well with the results in simulations of HS systems where critical crystal nucleation size is known to be less than a few hundred atoms.[15] Most of the results presented in this work

are performed using 500 and 3000 atoms. However, the finite size effect can no longer be neglected for systems with large disparity in the particle size ($\alpha < 0.2$) and small solvent concentration. The slow kinetics of the large sphere and their relative scarcity could make the crystallization process difficult. We shall encounter this issue in next section.

III. RESULTS

A. Identification of critical cooling rate

As discussed early, the glass formability of a glass-forming liquid can be defined as a set of optimal conditions that result in the critical cooling rate (CCR). The conditions are the aforementioned intrinsic material properties. Therefore, we can formally write the critical cooling rate q_C as a function of these parameters

$$q_C = f(\Delta H, \alpha, n, x_1, x_2, \ldots, x_{n-1}). \quad (2)$$

On the other hand, we define cooling rate operationally in our simulation as $q = d\varphi_0/d\tau$, where φ_0 is the initial packing density and τ stands for dimensionless time. q can be selected prior in our simulation as described in Sec. II [also see Fig. 1(a)]. Unlike an earlier definition[16] for the cooling rate Γ, the current definition q, is conveniently used in bidisperse and polydisperse mixtures.

In a binary hard sphere system, the relation shown in Eq. (2) is reduced to $q_C = f(\alpha, x_B)$. This simplification allows us to seek direct relation between the atomic size ratio and the cooling rate. Through a series of simulations with different q at each point at (α, x_B), we can locate the q_C. The critical cooling rate q_C is the one below which the first crystallization would occur. In other words, the CCR is the lowest cooling rate for a given glass-forming system.

It is worth to mention that in computer simulation, same as in real experiment, glass phase could always form if the cooling rate is sufficiently high. However, the CCR may not be attainable in many atomistic simulations because the small time scales dictated by the interatomic potentials ($\propto E^{-1/2}$, where E is the characteristic interatomic bonding energy) and the finite simulation times.[12,17] The time scale in the hard sphere system is not well defined, as E is zero. In addition, the dynamics in the hard sphere model is fast. Thus we could, with relative ease, identify CCR for our HS model system characterized by α and x_B.

The CCR is the property uniquely determined by the intrinsic material properties. The pure system ($\alpha = 1, x_B = 0$) has the highest CCR. As shown in Fig. 1(b), q_c of the one-component hard sphere system can be unambiguously identified using our adopted algorithm. This cooling rate can be used as a reference point for all alloy systems since the time in the hard sphere system is unitless. And thus direct comparison with experiments can be made with the relative, or normalized cooling rates using the CCR of the pure system as the reference. Note that the Lubachevsky-Stillinger (LS) algorithm[14,16] does not show a clear boundary between glass transition and crystallization as we compare their results with ours in Fig. 1(b). This is a crucial test for us in adopting our densification algorithm to determine CCR; and using LS algorithm, we may not be able to get CCR and accurately map out correct glass-forming diagram (see Fig. 3).

Furthermore, CCR is found insensitive to the system size difference between 500 and 20 000 spheres. Figure 1(c) shows the configurations obtained from densifications of 500, 3000 and 20 000 monosized spheres crystallized at their CCR's. The average q_C is found to be 0.0039 through these samples with a maximum variation of 10%. Even though CCR remains constant some differences are observed as the size of system increases. For example, a system with 500 spheres forms single crystal while systems with 3000 and 20 000 hard spheres form polycrystalline phases. Such a difference is also reflected in the equation of state for each system, as shown in Fig. 1(d): The drop of the pressure at the crystallization becomes much less and the pressure versus packing density becomes almost flattened out for larger systems. A horizontal line is expected for an infinitely large system. For practical purpose, therefore, small system is a better choice to detect possible crystallization.

As shown below, in binary HS systems the CCR depends sensitively on the atomic size ratio and shows a significant change as solute atoms are added to the host. As alloy elements of different diameters are added to the host of atoms, the critical cooling rate is expected to decrease. To obtain the critical cooling rate in the binary mixture, we prepared a series of samples that have different size ratios at a fixed concentration x_B of small atoms. We then quench or densify these samples with different initial quench rates q. Therefore, at a given solute concentration x_B, each simulation is characterized by two independent parameters, namely the size ratio α and the densification, or quench rate q. The final phase in each of the simulations is characterized and its packing density is calculated. The critical cooling rate is identified as the lowest cooling rate for each system before crystallization occurs. In the following, we show the quench process and the results for $q_C = f(\alpha, x_B)$ from three systems at $x_B = 0.1$, 0.20 and 0.3.

Figure 2(a) shows the phases obtained using various cooling rates and the critical cooling rate q_C, or CCR, for the system at $x_B = 0.2$. The vertical axis represents the final, or the steady state value of the packing density φ_m achieved by continuing simulations up to a large enough time. The packing density φ is defined as the ratio between the volume occupied by the atoms and the total volume of the system. Each vertical bar in Fig. 2(a) represents the location of each sample in the α-q parameter space and its height shows the corresponding value of the final packing density φ_m. The tip of each bar marked by either a filled circle or an unfilled circle represents crystalline and amorphous phase respectively.

The critical quench rate is identified in the diagram as the lowest cooling rate and it forms a boundary separating the crystalline phase and glass. A smooth boundary from the discrete number of simulations is determined using a curve-fitting tool in MATLAB.[18] The axis corresponding to q_C is in logarithmic scale in Fig. 2(b). The general trend is obvious, namely, at a given atomic size ratio, increasing quench or densification rate q leads to more disordered or glassy phase. Or with a given quench rate, decreasing the atomic size ratio (or increasing atomic size difference) leads to disorder or

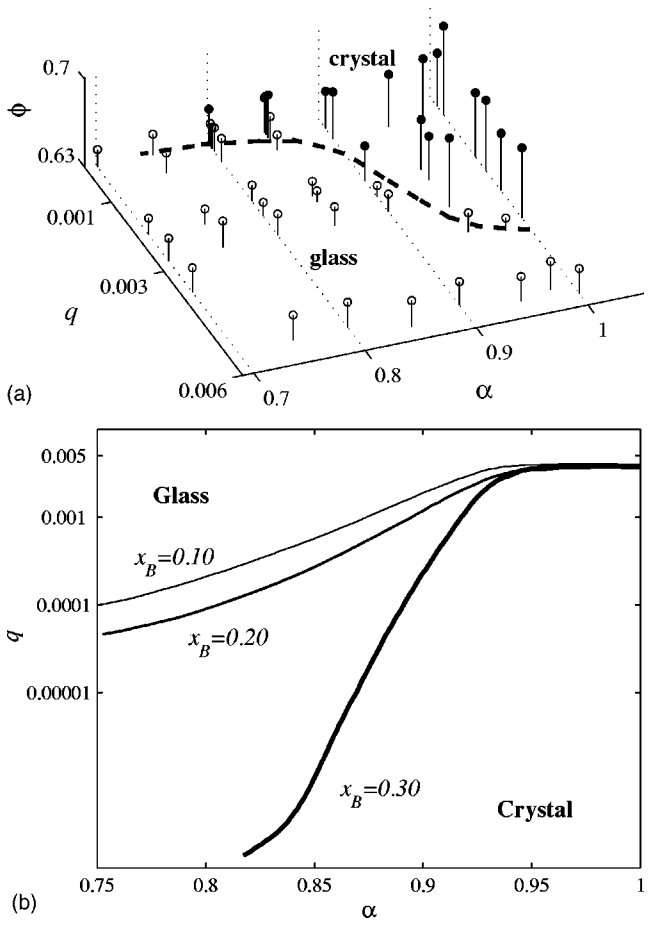

FIG. 2. (a) The quench rate versus atomic size ratio $(q-\alpha)$ for the binary mixtures with $x_B=0.20$. The vertical bar represents the final packing density φ_m. The CCR is shown as a dotted line. (b) The critical quench rates (CCR) versus atomic size ratio $(q-\alpha)$ for the binary mixtures with $x_B=0.10$, 20, and 0.30.

glass phase. Clearly, the glass formability, as represented by the cooling rate q_C differ for systems with varying α at different x_B. The GFA increases as the cooling rate decreases when α change from 1 for the pure system to 0.6 for the alloys. q_C drops the largest at $x_B=0.3$. As seen below, this trend of decreasing q_C or increasing GFA is related to the slowing down of the kinetics in the microstructure formation of the equilibrium crystal phases caused by atomic size difference.

It is interesting to notice that among the CCR's, some are the lowest for certain systems. As shown in Fig. 2, for the atomic size ratio $\alpha<0.85$, the CCR starts to level off for the system at $x_B=0.2$. It reaches a plateau in the range around $0.70<\alpha<0.80$. This lowest CCR (LCCR) is found to be $q_C\leqslant 5\times10^{-5}$ for $\alpha\approx0.80$, $x_B=0.20$ [Fig. 2(a)]. As a comparison, the LCCR for the pure system, which is the same as CCR, is $q_C^0\approx5\times10^{-3}$. q_C^0 is almost two orders of magnitude higher than that of the mixture.

The systems with the lowest critical cooling rate are the best glass formers. For our model systems with the alloy composition at $x_B=0.20$ they are those at the atomic sizes $0.70<\alpha<0.80$. For the systems at $x_B=0.30$ the LCCR is inaccessible for $\alpha<0.80$ (beyond which simulation time becomes excessively long). The CCR at $x_B=0.30$ are also the lowest among three systems tested ($x_B=0.1,0.2,0.3$). As shown later, the best GFA systems determined above coincide with the regions where the equilibrium phases are eutectic. The glass-forming liquids with these atomic size ratios can be cooled with the slowest cooling rate; In other words, glasses with the largest size can be made for these systems.[1,2]

The rendering of the relation, $q_C=f(\alpha,x_B)$, in the entire parameter space (α,x_B) would be desirable; but very time consuming. Some may not even be possible to obtain due to slow kinetics for crystallization (and finite simulation time). However, these systems usually have high solute concentrations, or extreme ratios of atomic sizes,[19] which are outside of the domain of interest for metallic alloys. An alternative way to obtain this relation $q_C=f(\alpha,x_B)$ is through contour plot shown below.

B. Glass-forming diagram

A kinetic phase diagram can be mapped out in the entire parameter space (x_B,α) to show a systematic view of glass and crystal phases, glass-forming regions, and glass formability. As noted early, any sufficiently high cooling rate can lead to glass formation. Therefore, unlike equilibrium phase diagram, in this kinetic phase diagram, cooling rate must be considered. This diagram can be obtained from simulations of the HS systems with different x_B and α at a given quench rate q accessible to our computing capability. In this case, instead of changing the cooling rate for each system at x_B and α as we did to identify the CCR, we change the parameters x_B and α at each preselected q. The boundary can, therefore, be obtained that marks the transition point between glass and crystalline phase [which is amount to mapping out the glass-crystalline phase transitions at a specific cooling rate q from the glass formability map (Fig. 2), $q=q_C=f(\alpha,x_B)$]. If a series of cooling rates are selected properly, a contour plot can be mapped out. The contour plot of the kinetic phase boundaries in x_B and α obtained from different q defines the glass-forming regions. Such a kinetic phase diagram is shown in Fig. 3.

Figure 3 shows the glass-forming region for a large range of the atomic size ratio and concentration (with 5 or 10 % interval for change in α and x_B) at three different applied cooling rates, corresponding to medium, slow and extremely slow cooling. They differ about five times from each other. The slowest one is taken as the CCR from the system with $\alpha=0.80$ and $x_B=0.20$ as shown in Fig. 2.

First, we notice that the glass-forming boundary of the mixtures in the range $0.7<\alpha<0.85$ is almost invariant to the change of cooling rate. At this range of α, the corresponding concentration for the glass-forming boundary is around $x_B=0.20$. Coincidently, the atomic size differences for the alloy composition are remarkably close to the critical values found by Hume-Rothery for crystalline solid solubility ($\alpha\leqslant0.85$).[20] As shown in a large number of real binary systems[20] the stable phases in the binary alloys beyond the Hume-Rothery atomic size limit are eutectic. Our results show that indeed, these systems with the highest stability (with almost invariant glass-crystal phase boundary shown in

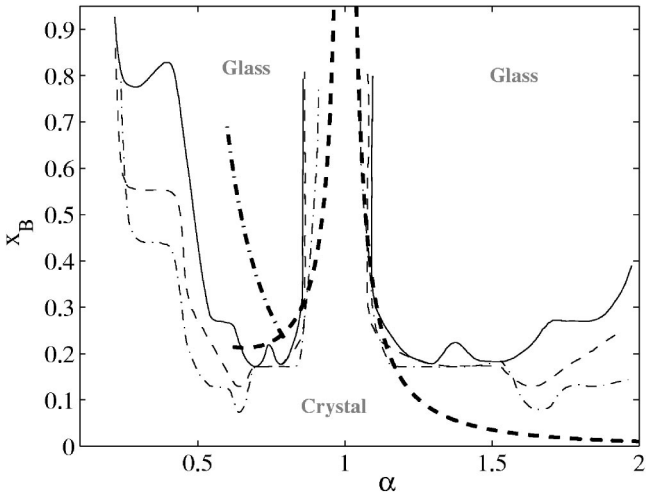

FIG. 3. The kinetic diagram for glass formation obtained at three different cooling rates represented by thinner lines. Solid line, dash line, and dotted-dash line stand for the cooling rates of $q_1=1.5\times10^{-5}$, $q_2=5.5\times10^{-5}$, $q_3=2.8\times10^{-4}$, respectively. As a comparison, results from Egami and Waseda (Ref. 7) (thick dash line) and Miracle and Senkov (Ref. 9) (thick dotted-dash line) models are also plotted. The areas representing glassy and crystalline regions are outlined in the figure.

Fig. 3) and best glass formability (among the slowest cooling rates shown in Fig. 2) have their crystalline counterpart of eutectic phase. This finding agrees with the well-known experimental observations.[21]

Figure 3 also shows agreement in general trend with Egami-Wadeda model[8] found in the range of $0.6<\alpha<0.80$ for the systems under the slowest cooling rate. However, large deviations from the model are found in the region of $\alpha>0.85$ and $x_B>0.30$. In this case, the glass-forming region is found to shift to smaller atomic size ratio ($\alpha<0.85$) in our simulations, while the Egami-Waseda calculation predicts the region bounded at $\alpha<0.95$. In fact, the glass-forming region predicted from the model is more in agreement with the glass-forming boundary at the fast cooling rate in our simulations. This is a key result pertinent to understanding the atomic mechanisms of atomic size effect on glass formation, and we shall return to it in the next section.

On the other hand, glass-forming boundary drastically changes with densification rate for $\alpha\leqslant0.65$. As seen from Fig. 3, the glass-forming boundary shifts toward higher x_B, while Egami and Waseda model [see Eq. (3) below] predicts a monotonically decreasing x_B as the atomic size ratio decreases. Even more drastic change is observed around the value $\alpha\sim0.40$. The boundary shifts abruptly to a much higher alloy concentration ($x_B\geqslant0.60$). Another abrupt change of the boundary is also observed at $\alpha\sim0.20$ where the minimum alloy concentration at the boundary of the glass forming region is shifted further up to $x_B\geqslant0.80$. The glass-forming region becomes narrower as the atomic size ratio decreases further ($\alpha<0.20$).

As shown in Fig. 3, the phase boundaries from our simulations differ also significantly from the prediction in a recent work[9] at the lower atomic size ratio ($\alpha<0.70$). As explained below, the large shift of the glass forming boundary toward higher alloy concentration x_B starting at $\alpha<0.75$ is caused by formation of different crystalline microstructures and intermetallics or compounds. A phase separation of two disordered fcc solid solutions occurs around $\alpha=0.75$.[19] This finding is fundamentally different from the mechanism proposed in Ref. 9, where homogeneous interstitial solid solution is assumed and become unstable and thus determining the glass-forming region boundary. The mechanism involving two competing crystalline phases were not anticipated in the early models.[7,9]

When the solute concentration becomes higher ($x_B>0.80$) we can consider the systems as mixing (a small amount of) large atoms into the host of the small ones. The atomic size ratio in this case is effectively greater than unity, or $\alpha>1$. For this reason, we plotted this portion of the diagram ($\alpha>1$) separately in Fig. 3. The boundary fits Egami-Waseda model in the region at $1<\alpha<1.1$ (Fig. 3). This is in a sharp contrast to the region with low solute concentration (the left side of the diagram with $\alpha<1$). We can explain this difference by the kinetics of the large atoms. The large atoms are less likely to move in the environment of small atoms. As a result, we found no detectable amount of microstructure forming (promoted by large atoms) in this region. However, as the atomic size difference becomes larger ($\alpha<0.50$ and $\alpha>1.2$), subtle microstructures start to form, that involve small atoms reorganizing themselves into ordered structures in the interstitials of the large atoms. In this region we also observed strong finite size effect on the microstructure and glass formation.[19]

The features reported above are observed for all three cooling rates. However, the magnitude of the change, or shifting of the glass-crystal phase boundary is different in different regions of α and x_B under different cooling rates. The largest shift of the boundaries at medium and high cooling rates are found for systems with $\alpha<0.70$ and $\alpha>1.2$. The glass-forming region expands with increasing cooling rate. Also, the expansion of the glass-forming region in systems with $\alpha>0.85$ becomes significant only at the high cooling rate. Under the medium cooling rate which is almost five times faster than the slowest one, the boundary does not shift much. At the high cooling rate, the phase boundary in this region moves very close to that predicted by Egami and Waseda.[7]

Only one part of the boundary, at $0.7<\alpha<0.85$, exhibits a remarkable resilience to changing cooling rate. As we mentioned early, this region corresponds to the eutectic composition of the binary hard sphere systems and has the best GFA. Finally, we found that the cooling rate shows relatively small effects on the phase boundaries in the high solute region ($\alpha>1$). As explained below, this is mainly due to the slow kinetics of the large sized atoms.

The contour plots at three different cooling rates also gives us a sketch of the CCR landscape, $q_C=f(\alpha,x_B)$: The CCR surface changes the fastest in the region $0.7<\alpha<0.95$ (and $\alpha<1.1$) and remains relatively flat in the region $0.70<\alpha$ (and $\alpha>1.2$). In the region close to $0.7<\alpha<0.85$ and $x_B\sim0.20$ the CCR surface exhibits an almost vertical drop. The contour plot with even lower cooling rates would give more details of the glass-forming property, especially in the regions in the middle of the phase diagram

($x_B \sim 0.50$ and $0.7 < \alpha < 0.85$). However, this is beyond our computational capability.

C. Packing instability

Glass formation induced by atomic size difference is often rationalized from the point of view of crystal (packing) instability:[7] If crystal(s) cannot form due to packing instability in a system made of different sized atoms, a glass will form. An example of this argument is the solid-state amorphization (SSA) where glasses do form through direct destabilization of crystals.[22,23] This atomic-size-induced instability was originally proposed by Hume-Rothery to predict phase formation in binary systems.[12]

As argued by Hume-Rothery, when small atoms are mixed with large ones, the host made of the large atoms can dissolve certain amount of small atoms by accommodating them in the lattice site if the size difference is smaller than a critical value. (This applies too to mixing large atoms into small atom host.) Further increase in atomic size difference causes increase in the strain energy in the host due to the size disparity. If this energy increase becomes large enough, it would drive the solution into different phases, most likely eutectics as we see from most of the Hume-Rothery alloys that follow the rule.[20,24] This critical size, or Hume-Rothery limit is at $\alpha \sim 0.85$. Egami-Waseda model extended Hume-Rothery theory by including local topological instability induced by atomic size difference. Unlike the phase transitions observed in Hume-Rothery alloys, this model imposes a restriction of polymorphism; and as a result, the final phase predicted from the model is either a crystal or glass, both of which are single phase with the same (local) chemical composition.

There are several key questions that have not been addressed in the instability theories for glass formation. (1) How is the packing instability relevant when a liquid is cooled, or how the CCR observed in quenching the glass-forming liquid connects to the packing instability or glass formation? (2) What are the roles in glass formation played by competing crystalline phases which could form under the same instability conditions, or if the polymorphic constraint is no longer valid? In the following, we shall probe these questions from a different angle in the HS system.

Since there is no attractive interaction, phase stability and thermodynamic properties in hard sphere systems are dominated by packing density. The maximum achievable packing density in binary mixtures depends on atomic size ratio and relative solute atom concentration. We can estimate the packing density of a binary mixture made by mixing smaller atoms uniformly with the large ones to form a random substitutional fcc solid solution. (For the pure hard sphere system, fcc packing is the equilibrium structure with the highest packing density.) Its packing density can be readily calculated as a function of x_B and α (Ref. 25),

$$\varphi_{\mathrm{fcc}}^{b} = \frac{\pi}{3\sqrt{2}}[1 - x_B(1 - \alpha^3)], \tag{3}$$

where $0.5 \leqslant \alpha \leqslant 1$ and $0 \leqslant x_B \leqslant 0.5$. Equation (3) is plotted for $x_B = 0$ (pure system) and $x_B = 0.20$ (binary mixture) in Fig. 4. This equation gives the exact result in the pure system corresponding to $x_B = 0$ and $\alpha = 1$. In the same figure, we also plot the maximum, or final packing densities φ_m and $\varphi_{\mathrm{fcc}}^{b}$ for glasses and fcc solid solutions from our simulations. The lower packing density for the pure system and binary fcc mixture, or solid solution from the simulations is a result due to the presence of defects, grain boundaries, or nonuniform distribution of atoms [see Fig. 1(c)].

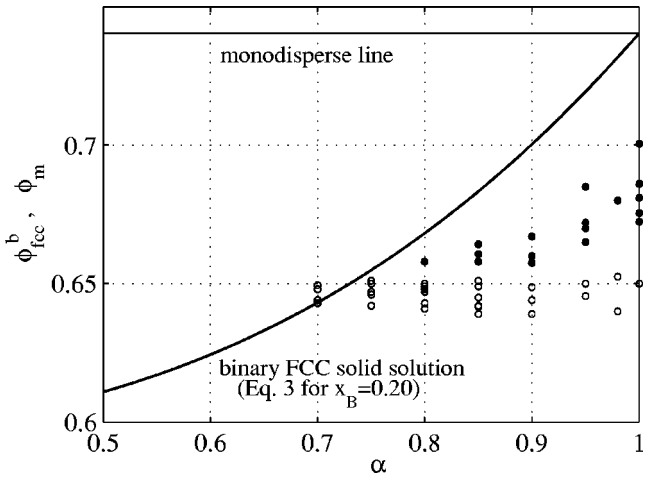

FIG. 4. Variation of $\varphi_{\mathrm{fcc}}^{b}$ with α for a pure ($x_B = 0$) and binary system ($x_B = 0.20$). Packing densities obtained from simulations are also shown: Filled circles represent the fcc binary solid solution and open circles represent the amorphous phase. Multiple symbols at the same α represent packing densities of the same system under different quench rates.

Equation (3) shows that $\varphi_{\mathrm{fcc}}^{b}$ decreases monotonically as α moves to smaller size ratios. If we allow $\varphi_{\mathrm{fcc}}^{b}$ take values at smaller α, we will soon run into a dilemma: The packing density $\varphi_{\mathrm{fcc}}^{b}$ of the mixture with fcc structure will become smaller than the packing density of a glass. In other words, the mixture will be more stable if it collapses into a disordered state that has a higher packing density. The crossover point in the packing density from fcc to a disordered but denser phase signals a possible phase transition (order-to-disorder or crystal-to-glass transition).

The critical value for α can be found at which the packing density of the fcc mixture equals that in the disordered, glassy state. From the simulation results shown in Fig. 4, we can see that the critical value for this transition occurs at $0.75 < \alpha_C < 0.80$ for $x_B = 0.20$. The upper bound at $\alpha_C = 0.80$ coincides with α at the boundary of the best glass-forming region obtained using the LCCR in the quenching process (Fig. 3).

We can also estimate the critical limit for α directly from Eq. (3). If we assume that the glass transition occurs when the packing density of the crystalline mixture reaches that of the glassy phase, or $\varphi_{\mathrm{fcc}}^{b} = \varphi_{\mathrm{glass}} = 0.65$, the critical size ratio $\alpha_C = 0.73$. This estimate is slightly lower than the values obtained from simulations ($0.75 < \alpha_C < 0.80$). The discrepancy between these two critical atomic size ratios comes from difference in $\varphi_{\mathrm{fcc}}^{b}$ in Eq. (3) and simulations. In Eq. (3) we assume a perfect fcc structure while in simulation, various disorder may be present [see Fig. 1(c)]. The later will lower

the values of $\varphi_{\mathrm{fcc}}^{b}$ and thus raise the estimated critical value of atomic size ratio α_C in our simulation results in Fig. 4.

From these results and Eq. (3), we can, therefore, obtain a formal relation between the minimum alloy concentration x_B and the atomic size ratio α, which marks the boundary of the glass-forming region

$$x_B^{\min} = \frac{1 - 3\sqrt{2}\varphi_{\mathrm{fcc}}^{*b}/\pi}{|1-\alpha^3|} = \frac{A}{|1-\alpha^3|}. \tag{4}$$

The glass-forming region is defined at $x_B \geqslant x_B^{\min}(\alpha)$. The coefficient in Eq. (4), $A = 1 - 3\sqrt{2}\varphi_{\mathrm{fcc}}^{*b}/\pi = 1 - \varphi_{\mathrm{fcc}}^{*b}/\varphi_{\mathrm{fcc}}$, where $\varphi_{\mathrm{fcc}} = \pi/3\sqrt{2} = 0.74$ is the packing density of a pure fcc phase. $\varphi_{\mathrm{fcc}}^{*b}$ is the critical packing density of the metastable fcc solid mixture at the onset of the instability. For an estimate, we let $\varphi_{\mathrm{fcc}}^{*b}$ equal the packing density of the glass phase φ_{glass} and $\varphi_{\mathrm{fcc}} = 0.74$. Then $A = 0.122$ if we substitute the packing density for the amorphous phase $\varphi_{\mathrm{glass}} = 0.65$ for $\varphi_{\mathrm{fcc}}^{*b}$. If we use the value for φ_{fcc} from our simulation (Fig. 4), $\varphi_{\mathrm{fcc}} = 0.70$, we have $A = 0.07$. The phase boundaries estimated using Eq. (4) with $A = 0.7$ agree very well with our simulation results in the range of $0.7 \leqslant \alpha < 0.85$ (see Fig. 4).

A similar relation [Eq. (4)] was derived by Egami and Waseda.[7] The coefficient A was estimated to be 0.1 in their work.[7] Our results presented above show that A is generally not a constant. It is a function of the atomic size ratio through the packing density $\varphi_{\mathrm{fcc}}^{*b}$ which is dependent of α (and x_B as well).[19] Note also that Eqs. (3) and (4) are applicable to the systems where the ground state, or the host is the fcc phase.

In deriving Eq. (4), and also in the model by Egami and Waseda, a polymorphic constraint is imposed: There is no alloy concentration change allowed. On atomic scale, we assume that alloy elements are not allowed to move beyond the first neighbor shell once they occupy fcc lattice positions. Clearly, this constraint is not valid in a glass-forming liquid when it is cooled toward undercooled region. Atoms do have time to move through diffusion, unless the cooling rate is infinitely fast, or at least faster than that determined by the characteristic diffusion time of the system. Therefore, the instability theories of the hard sphere model [Eq. (4)] and Egami-Waseda model are only valid for high cooling rate. This conclusion is corroborated by our simulation results (Fig. 3).

(1) As mentioned early, in simulation the glass-forming boundary in the region of $\alpha > 0.85$ shifts to the right as the cooling rate increases, and become closer to the theoretical boundary predicted by Egami and Waseda. The boundary in $\alpha > 1.2$ shifts upwards. In both cases, the glass forming regions are larger in the instability models than those from our simulations, and are closer to the simulated boundaries with high cooling rate.

(2) For the glass-forming systems at $\alpha < 0.75$, the best glass formers are those mapped out by our simulations since they are obtained using the slowest cooling rates. The glass-forming boundary predicted from Eq. (4) is below this curve. In fact, we can make the crystal-glass phase boundary in this region to follow exactly the predicted relation. But the cooling rates in the simulation at each point along this boundary will be different and also much higher.[13] The reason for this discrepancy (or the upward swing of the boundary as α decreases) is the formation of two disordered fcc phases with different solute concentrations,[19] which is not considered in Eq. (4) and the Egami-Waseda model. We shall return to this point in next section with more details. Therefore, we could conclude that the instability criteria are not suitable for predicting glass formability, as they only apply when cooling rate is extremely high; while to predict glass formability, it is the slowest cooling rate that matters.

IV. DISCUSSIONS

How atomic size difference affects glass formation has been an outstanding problem in materials science and glass synthesis. Using a hard sphere model, we were able to simplify the issue to a relation involving only atomic size ratio and relative alloy concentration in binary systems. This model system makes it possible to see how the critical cooling rate of a glass-forming liquid is related to the atomic size difference. We need to stress here that this relation does not necessarily predict the glass formability for real binary alloys or mixtures (direct reference can, however, be made in systems exhibiting hard-sphere-like characteristics, such as colloidal particles, granular matter, and rocks); instead, it shows us what the glass formability should look similar to if it is affected by atomic size difference alone. Modifications to the kinetic diagram for the glass formation would occur once other factors, especially the heat of mixing, or attractive interatomic interactions, are considered.[27] Nevertheless, this relation (Fig. 3) is expected to provide a useful reference for atomic size effect if different atoms, or particles are considered for making bulk metallic glasses or colloidal glasses.

This work focuses mainly on characterizing phenomenology using computer simulations of glass formation and glass formability as a function of atomic size difference, including the critical cooling rate and glass formability (Sec. III A), kinetic glass formation diagram (Sec. III B), and packing instability of mixtures (Sec. III C). There are also results that have not been presented in detail in this paper, but are important for understanding the observed phenomena. In the following, we shall briefly summarize them:

Competing microstructures. As mentioned in Sec. III B, the phase boundary for the glass formation region shifts to higher value at $\alpha < 0.75$ (also at $\alpha > 1.2$). This and other parts of the kinetic phase diagram are closely related to the formation of various microstructures and crystalline phases.[19] A brief summary of the crystalline phases observed in our simulation is listed below.

(1) In the range of $0.5 < \alpha < 0.75$, we observe local clustering of the same type of atoms (Fig. 5). This phenomenon is more pronounced in the binary systems of small atoms mixed into the host of large atoms ($\alpha < 1$) than that in the systems with large atoms mixed into small host atoms ($\alpha > 1$). (2) In the region around $\alpha \sim 0.40$, an intermetallic phase form that consists of the large atoms occupying the regular fcc lattice and the small atoms sit in the octahedral interstitial sites (Fig. 6). The glass formation becomes possible only after all octahedral sites are occupied, or the mini-

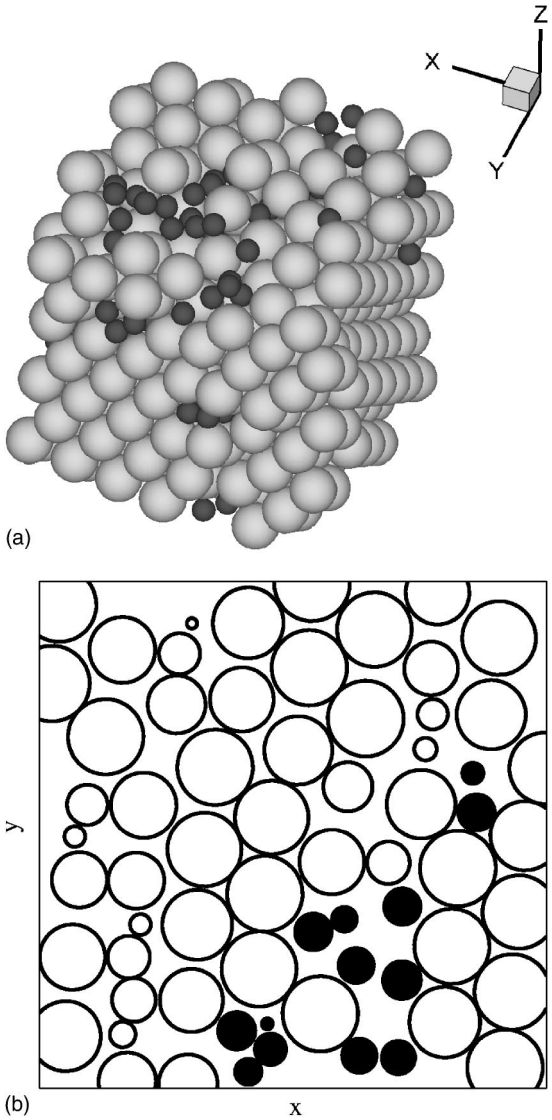

FIG. 5. The atomic structure of a sample with 500 atoms with $\alpha=0.50$, $x=0.25$. The large spheres and small black spheres represent the large atoms and the small atoms, respectively. To show the local clustering of the small atoms, a cross section in the *xy* plane of the sample is shown. The filled circles represent small solute atoms. The crystalline order of the large atoms in this cross section is clearly seen. The diameters of the circles in the cross section are not in direct proportion to the diameters of the atoms due to the cut.

mum concentration of the small atoms is larger than 0.5 (see Fig. 3). (3) For systems with slightly larger size ratio, $0.41<\alpha<0.5$, we found very small number of octahedral sites occupied by small atoms. Disordered fcc packing is abundant. This is not a surprising result since interstitial solid solution is very difficult to form due to the exceedingly high energy even when atomic size mismatch does not deviates much from the octahedral interstitial ratio ($\alpha=0.41$). Correspondingly, we see that the phase boundary in Fig. 3 rises steeply in $0.4<\alpha<0.5$. (4) In the region around $\alpha\sim0.20$, we observe the formation of another intermetallics with large atoms occupying the fcc lattice and small atoms occupying the octahedral sites. In this case, small atoms, usually a

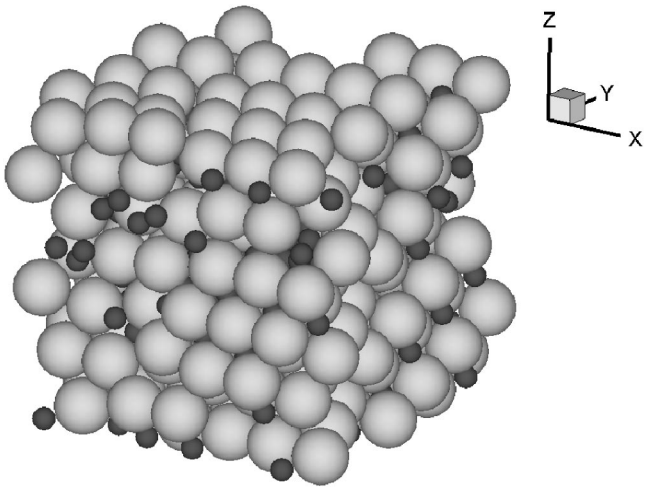

FIG. 6. Atomic structure of a sample with 500 atoms at $\alpha=0.40$ and $x=0.50$. It forms octahedral interstitial solid solution and interstitial compound. Small atoms are shown to occupy octahedral interstitials and a periodic arrangement of small atoms is shown.

group of them ranging from two to four or six, occupy the same octahedral site. (5) For $\alpha>1.2$, the same trend of upward shift of $x_B^{\min}$ is observed. However, the magnitude is smaller than that at $\alpha<0.75$. The main mechanism underlying this trend is the local concentration change due to clustering of small atoms.

These findings clearly demonstrate that the atomic size difference affect glass formability directly through the formation of competing microstructure or crystalline phases. The same driving force (or energy increase in an interacting system) caused by atomic size difference, which are expected to lead to crystal packing instability, could also lead to either composition change or crystalline phase formation in the glass-forming *liquid*. For the former case, the polymorphic constraint no longer holds. For the later case, due to the different crystalline phases, the mechanisms of the glass formability could be quite different. In both cases, the reference local (crystalline) packing is different in local chemical composition or topology from the local packing in the instability theory[7,8] that has the same local chemical concentration as the mean alloy concentration or just one local crystal structure.

For a given cooling rate q, the liquid has a time scale determined by the cooling rate $\tau\sim1/q$. On the other hand, the system have characteristic time scales for forming different crystalline phases or microstructures, $\tau_1,\tau_2,\ldots\tau_n$, where n is the number of possible crystalline phases and microstructures. These different time scales are determined by specific crystalline phases that would form either in equilibrium or metastable states. Glass formation becomes possible only when these competing processes are removed. This requires that the time scale for cooling the glass-forming liquid, $\tau<\min\{\tau_1,\tau_2,\ldots,\tau_n\}$ or $q>\max\{1/\tau_1,1/\tau_2,\ldots,1/\tau_n\}$. On the other hand, glass formability, as characterized by CCR, is uniquely determined by the shortest characteristic time scale among $\tau_1,\tau_2,\ldots,\tau_n$. The critical cooling rate is $q_c=\max\{1/\tau_1,1/\tau_2,\ldots,1/\tau_n\}$. Therefore, the critical cooling

rate or glass formability is determined directly by what the competing crystalline phase or microstructure is out there for a given system. As shown above, these competing phases are quite different in our model system. The detailed mechanisms of how the crystalline phases form leads to the time scales $\tau=\min\{\tau_1,\tau_2,\ldots,\tau_n\}$, and the CCR.

For the systems at $\alpha\sim0.40$, the small alloy atoms are fast diffusers in formation of the interstitial solid solution and interstitial compound.[19] The CCR for this system is, therefore, determined by the formation of these *two* phases. This crystallization process could be slowed down when the available interstitial sites are taken, that is, only when the solute concentration is high. The excess number of solute atoms in the liquid has to diffuse a long way to form a single component fcc phase (or fcc solution with small amount of large atoms), which prolong the characteristic time τ. Indeed, the glass-forming boundary for this system is moved up to $x_B\geqslant0.50$ where the lowest CCR are found. As a comparison, the glass-forming boundary around the region of $0.75<a<0.85$ is much lower, $x_B\sim0.20$. The reason for this is that the competing crystalline microstructure in this range of α is a eutectic mixture. It consists of two (disordered) fcc solid solutions, one with large atom as the solvent and another with small atoms as solvent.[19] In order to form the eutectic mixture, long-range diffusion of both small and large atoms are needed, which has much longer time scale as compared with that for the small atoms to diffuse to form the interstitial compound at $\alpha=0.40$. Thus the cooling rate is lower, and the glass formability is higher at much lower x_B.

In neither of the above cases is the polymorphic constraint obeyed: variation of local chemical concentration occurs; and there are multiple competing crystal structures as well. The instability model, on the other hand, demands that the composition remain homogeneous microscopically and the two disordered fcc phases are not considered either.

Applicability of the crystal packing instability models. Following the argument put forward above, we see that the crystal packing instability models can only treat a rather special case where the transition between glass and crystalline phase is polymorphic. In general, maintaining this constraint demands high cooling rate ($q=q_{\text{instability}}$) in order to suppress competing crystalline phases and local chemical composition variations.[26] Therefore, the glass formability determined by this cooling rate does not reflect the intrinsic material property. In general, $q_{\text{instability}}\geqslant q_c=\max\{1/\tau_1,1/\tau_2,\ldots,1/\tau_n\}=f(\Delta H,\alpha,n,x_1,x_2,\ldots,x_{n-1})$ if competing crystalline phases exist, or alloy composition can change, including short-range ordering or clustering. In other words, the glass formability derived from the instability models is the fastest cooling rate, not the CCR used to characterize the GFA.

V. CONCLUSIONS

Using a binary hard sphere model, we are able to investigate the relationship between the atomic size difference and the critical cooling rate and glass formation. Through extensive molecular dynamics simulations, we identified the critical cooling rates for the systems and their relations with the atomic size difference. We also obtained the boundary of the crystallization and the best glass-forming region. We defined the glass formability as a set of optimal conditions involving intrinsic material properties that lead to slowest cooling rate or CCR of the material system. Both the conceptual developments and computational efforts enable us to study quantitatively the atomic size effect on glass formability. As a result, a glass formability map or a kinetic phase diagram is mapped out that identify the glass formability and regions of glass and crystalline phases at different cooling rates.

We found that the glass formability is closely related to the formation of crystalline phases and other microstructures. The mechanisms of the best glass formation are different, depending on what and how the competing crystalline phases form. Therefore, the glass formability is different for different systems with different intrinsic material properties. This conclusion manifests in the four different glass-forming regions marked by different atomic size ratios. The potency of atomic size difference in the different regions is, therefore, quite different. It diminishes as the competing crystallization emerges.

The results obtained from the simple hard sphere system have clearly demonstrated that glass formability is an intrinsic material property necessarily connected to crystal formability. This conclusion provides a direct support, albeit in a numerical model, for Turbull's proposal[1] that the best glass (or highest glass formability) can be obtained only when crystalline phase(s) cannot form. Furthermore, we learned that the instability models are incapable of predicting glass formability (not the glass formation) due to the strict kinetic constraint.

ACKNOWLEDGMENTS

The authors would like to acknowledge the financial support for this work provided by the National Science Foundation (Grant No. NSF0296163) and the Structural Amorphous Metals Program of DARPA under ARO Contract No. DAAD19-01-1-0525. M.L. would like to thank the Army Research Laboratory (ARL) for providing financial support at the early stage to initiate this work and J. S. Poon and G. Shiflet for many stimulating discussions.

[1] D. Turnbull, Sci. Am. **212**, 38 (1965); D. Turnbull, Contemp. Phys. **10**, 473 (1969).
[2] A. Paker and W. L. Johnson, Appl. Phys. Lett. **63**, 2342 (1993).
[3] Z. P. Lu and C. T. Liu, Phys. Rev. Lett. **91**, 115505 (2003).
[4] F. Q. Guo, S. J. Poon, and G. J. Shiflet, Mater. Sci. Forum **331–333**, 31 (2000).
[5] G. Shiflet, Science **300**, 443 (2003).
[6] S. H. Liou and C. L. Chien, Phys. Rev. B **35**, 2443 (1987); F. Q.

Guo, S. Enouf, G. Shiflet, and S. J. Poon, Mater. Trans., JIM **41**, 1406 (2000).
[7] T. Egami and Y. Waseda, J. Non-Cryst. Solids **64**, 113 (1984).
[8] T. Egami, Mater. Sci. Eng., A **226**, 261 (1997).
[9] D. B. Miracle and O. N. Senkov, Mater. Sci. Eng., A **347**, 50 (2003).
[10] M. P. Allen and D. J. Tildesley, *Computer Simulation of Liquids* (Oxford University Press, London, 1987).
[11] S. Miller and S. Luding, J. Comput. Phys. **193**, 306 (2004).
[12] P. Jalali and M. Li (unpublished).
[13] R. J. Speedy, F. X. Prielmeier, T. Vardag, E. W. Lang, and H. D. Ludemann, Mol. Phys. **62**, 509 (1987); M. J. Maeso, J. R. Solana, J. Amoros, and E. Villar, J. Chem. Phys. **94**, 551 (1991); M. D. Rintoul and S. T. Torquato, *ibid.* **105**, 9258 (1996).
[14] B. D. Lubachevsky and F. H. Stillinger, J. Stat. Phys. **60**, 561 (1990).
[15] B. O'Malley and I. Snook, Phys. Rev. Lett. **90**, 085702 (2003).
[16] T. M. Truskett, S. Torquato, and P. G. Debenedetti, Phys. Rev. E **62**, 993 (2000).
[17] The time scales in most systems with continuous interatomic interaction are of the order of $10^{-(12-13)}$ s. A typical MD run of 10^6 time steps to cool a liquid at 10^{2-3} K to a glass state at 10 K only leads to a cooling rate of 10^{8-10} K/s. If the critical cooling rate is decreased by several orders of magnitude in alloys or mixtures, as we see in the hard sphere system, the MD simulation time needs to increase accordingly, which may not be achieved easily. For the hard sphere system, this restriction may not be fatal: The time scale is defined arbitrarily and the critical cooling rate for crystallization is relatively high. Therefore, one can identify the critical cooling rate effectively with roughly 10^{6-7} collisions which are achievable with modern computers. However, exception may still occur when kinetic of crystallization becomes extremely slow (as in eutectic systems).
[18] A curve-fitting toolbox of MATLAB is used for curve fitting purpose. More details can be found in: *Neural Network Toolbox User's Guide*, The MathWorks, 1992–2001.
[19] P. Jalali and M. Li, Intermetallics **12**, 1167 (2004).
[20] W. Hume-Rothery, *The Structure of Metals and Alloys* (Institute of Metal, London, 1944).
[21] A. Inoue and A. Takeuchi, Mater. Trans., JIM **43**, 1892 (2002); D. Ma, Y. Zhang, H. Tan, and Y. Li, Mater. Sci. Forum **426–4**, 1945 (2003).
[22] W. L. Johnson, Prog. Mater. Sci. **30**, 81 (1986).
[23] M. Li, Phys. Rev. B **62**, 13979 (2000).
[24] *Binary Alloy Phase Diagrams*, edited by T. B. Massalski, J. L. Murray, and L. H. Bennett (American Society for Metals, Metals Park, Ohio, 1986).
[25] Suppose that spheres of small diameter d_B are uniformly distributed in the fcc lattice of large spheres of the diameter d_A. The small atom concentration is x_B and the atomic size ratio is $\alpha = d_B/d_A$. We assume that the two parameters are limited to $0.5 \leqslant \alpha \leqslant 1$ and $0 \leqslant x_B \leqslant 0.5$. (Outside of these limits, the following formulation may not be appropriate.) The equilibrium length of each side of the unit fcc cell equals $\sqrt{2}d_A$. The volume of the fcc unit cell is $V_c = 2\sqrt{2}d_A^3$. Since the number of atoms in an fcc unit cell is 4, we can assume that the average number of the lattice sites occupied by the small atoms is $4x_B$. Therefore, the volume occupied by all atoms belonging to the unit cell can be written in average as $V_s = 2\pi(x_B\alpha^3 + 1 - x_B)d_A^3/3$. This estimation is written based on a uniform distribution of small atoms among the large ones and the concentration of small atom is less than 0.5. Therefore, the packing density of the fcc mixture that is defined as $\varphi_{\mathrm{fcc}}^b = V_s/V_c$ leads to Eq. (3).
[26] *Science and Technology of Rapid Solidification and Processing*, edited by M. A. Otooni (Kluwer, New York, 1994).
[27] H. J. Lee, T. Cagin, W. A. Goddard, and W. L. Johnson, J. Chem. Phys. **119**, 9858 (2003).